

The Limits of Cosmic Shear

Thomas D. Kitching^{1*}, Justin Alsing^{2,3}, Alan F. Heavens², Raul Jimenez^{4,5},
Jason D. McEwen¹, Licia Verde^{4,5}

¹*Mullard Space Science Laboratory, University College London, Holmbury St Mary, Dorking, Surrey RH5 6NT, UK*

²*ICIC, Astrophysics, Imperial College, Blackett Laboratory, Prince Consort Road, London SW7 2AZ, UK*

³*Center for Computational Astrophysics, 160 5th Ave, New York, NY 10010, USA*

³*ICC, University of Barcelona, IEEC-UB, Marti Franques, 1, E08028 Barcelona, Spain*

⁴*ICREA, Pg. Lluis Companys 23, 08010 Barcelona, Spain*

ABSTRACT

In this paper we discuss the commonly-used limiting cases, or approximations, for two-point cosmic shear statistics. We discuss the most prominent assumptions in this statistic: the flat-sky (small angle limit), the Limber (Bessel-to-delta function limit) and the Hankel transform (large ℓ -mode limit) approximations; that the vast majority of cosmic shear results to date have used simultaneously. We find that the combined effect of these approximations can suppress power by $\gtrsim 1\%$ on scales of $\ell \lesssim 100$. A fully non-approximated cosmic shear study should use a spherical-sky, non-Limber-approximated power spectrum analysis; and a transform involving Wigner small-d matrices in place of the Hankel transform. These effects, unaccounted for, would constitute at least 11% of the total budget for systematic effects for a power spectrum analysis of a Euclid-like experiment; but are they are unnecessary.

Key words: Cosmology: theory – large-scale structure of Universe

1 INTRODUCTION

Weak lensing is the phenomenon whereby the images of distant galaxies are distorted by the effect of gravitational potentials caused by matter perturbations along the line-of-sight. This gravitational lensing effect induces a small change in the ellipticity¹ of a galaxy’s image known as shear. The shear caused by the large-scale structure of the Universe is known as ‘cosmic shear’. The mean of the complex cosmic shear field is zero but its 2-point correlation function or power spectrum contains cosmological information; cosmic shear is also used as a synonym for this statistic. This statistic is a particularly sensitive probe of dark energy because it measures the power spectrum of matter overdensity perturbations across large portions of the expansion history of the Universe. Because of this there are several on-going wide-field surveys that attempt to measure this effect, for example CFHTLenS (Heymans et al., 2012), DES (The DES Collaboration et al., 2015), DLS (Jee et al., 2015), KiDS (Kuijken et al., 2015), and HyperSuprimeCam; as well as several more planned surveys, for example *Euclid*² (Lau-reijs et al., 2011), LSST (LSST Science Collaboration et al., 2009), and *WFIRST* (Spergel et al., 2015), that have the

measurement of this statistic as one of their primary science goals.

In practice there are several ways in which the cosmic shear 2-point statistic can be computed that can be broadly categorised into real/configuration-space measurements as a function of celestial angle (e.g., shear correlation functions), and angular spherical-harmonic/Fourier-space measurements (e.g., power spectra). Furthermore these statistics can be computed in a series of redshift bins, to capture the geometry of the three-dimensional shear field, an approach known as ‘tomography’; or a spherical-Bessel/Fourier-space measurement in the radial direction known as ‘three-dimensional’ cosmic shear (Heavens, 2003, Castro et al., 2005, Kitching et al. 2007).

In this paper we present each of the primary approximations in cosmic shear statistics and explicitly link all of the currently used statistics together into a general schema. In doing so we also present a general three-dimensional spherical-radial statistic which is the redshift-space equivalent of a spherical-Bessel analysis. We discuss various approximations and a data compression, namely: flat-sky, Limber, tomography and Hankel transformations. The flat-sky assumption projects onto a locally flat tangent plane on the sky. The tomographic data compression, presented in Hu (1999), is a lossy binning of the cosmic shear signal into several redshift bins and is an approach used by *all* cosmic shear studies (see Kilbinger, 2015 for a review) except

* t.kitching@ucl.ac.uk

¹ Third flattening, or third eccentricity.

² <http://euclid-ec.org>

those that use a spherical-Bessel representation (e.g. Kitching et al. 2014), for both theoretical studies and data analysis. In Kitching, Heavens, Miller (2011) and Kitching et al. (2014) it was shown how to derive the tomographic case from a more general spherical-Bessel representation of the shear field. The Limber approximation links angular and radial wavenumbers together via a comoving distance relation. This was first discussed in Kaiser (1998) in the context of cosmic shear and has been investigated in Kitching, Heavens, Miller (2011) in cosmic shear studies, but in the majority of theoretical studies and data analyses it is an assumption. There is a particularly clear illustration of the Limber approximation in LoVerde & Afshordi (2008) that we discuss in this paper.

Most of the approximations we investigate are used simultaneously and in combination. Notably all the primary cosmological results from all of the wide-field surveys use a flat-sky, tomographic, Limber-approximated correlation function analysis, e.g., Heymans et al. (2013) for CFHTLenS; The DES Collaboration et al., (2015) for DES; Jee et al. (2015), and Hildebrandt et al. (2016) for KiDS. Notable exceptions include Pen et al. (2002), Brown et al. (2003), Heymans et al. (2005), Köhlinger et al. (2016), Alsing et al. (2016b), and the Po1Spice measurements in The DES Collaboration et al., (2015), all whom used Fourier-space measurements in angle, with the flat-sky, tomographic and Limber approximations. In Kitching et al. (2007) and Kitching et al. (2014) a flat-sky spherical-Bessel analysis was used without the tomographic or Limber approximations.

This paper is presented in the following manner. In Section 2 we review the cosmic shear formalism starting with the spherical-Bessel representation and then present the spherical-radial and correlation function representations. In Section 3 we discuss the flat-sky, tomographic and Limber approximations and present a general schema for linking these statistics and approximations. We discuss the implications of this for current results in Section 4. We discuss conclusions in Section 5.

2 COSMIC SHEAR METHODS

We begin by introducing several versions of the two-point cosmic shear statistic that treat the data, and represent the underlying three-dimensional shear field, in different ways. The first of these is the spherical-Bessel representation that has been described in detail in Heavens (2003); Castro, Heavens, Kitching (2005); Heavens, Kitching, Taylor, (2006); Kitching (2007); Kitching, Taylor, Heavens, (2008); Kitching, Heavens, Miller (2011); Kitching et al. (2007); Kitching et al. (2014), the second is the presentation of a spherical-radial representation of which the commonly used tomographic statistic (Hu, 1999) is a simple approximation. We then discuss real/configuration-space representations.

2.1 The Spherical-Bessel Representation

The cosmic shear field has spin-weight 2, and we can perform a spherical-Bessel transform to obtain

$$\gamma_\ell^m(k) = \sum_g \gamma_g(r_g, \theta_g) j_\ell(kr_g) {}_2Y_\ell^m(\theta_g) \quad (1)$$

where the sum is over all galaxies g at three-dimensional comoving coordinates (r_g, θ_g) , k is a radial wavenumber and ℓ is an angular wavenumber. The $j_\ell(kr_g)$ are spherical Bessel functions. The ${}_2Y_\ell^m(\theta_g)$ are spin-weight 2 spherical harmonics. Such a sum can be used to construct the data vector for a spherical-Bessel analysis of weak lensing data, which is then compared with the following theoretical covariance, as described in Kitching et al. (2014). When applying this sum to data these transformed coefficients can be manipulated to extract the pure E and B-mode signals (where cosmic shear is only expected to produce an E-mode signal), and remove any multiplicative measurement biases (where the measured γ_g is related to the true γ_g^T via some linear relation $\gamma_g = (1 + m)\gamma_g^T$, where m is an estimated bias parameter) as described in Kitching et al. (2014). The sum over galaxies is an estimator for a continuous integral over angle and radius, where there is an additional shot-noise contribution to the covariance, due to having a finite number of galaxies at discrete points (see Heavens, 2003).

The mean of equation (1) is zero, but the covariance of the transform coefficients is non-zero. Assuming isotropy the covariance of the harmonic coefficients – known as the power spectrum – can be written as

$$\langle \gamma_\ell^m(k) \gamma_{\ell'}^{m'}(k') \rangle = C_\ell^{SB}(k, k') \delta_{\ell\ell'} \delta_{mm'}. \quad (2)$$

Using the notation of Kitching, Heavens, Miller (2011), we can write down the theoretical expectation value of the power spectrum for given a cosmology

$$C_\ell^{SB}(k, k') = |D_\ell|^2 \mathcal{A}^2 \int \frac{d\tilde{k}}{k^2} G_\ell^{SB}(k, \tilde{k}) G_\ell^{SB}(k', \tilde{k}), \quad (3)$$

where the pre-factor $\mathcal{A} = 3\Omega_M H_0^2 / (2\pi c^2)$ (where H_0 is the current value of the Hubble parameter, Ω_M is the ratio of the total matter density to the critical density, and c is the speed of light in a vacuum). The variable $|D_\ell| = \sqrt{(\ell + 2)! / (\ell - 2)!}$ in the spherical case (see Castro et al., 2005; and Leistedt et al., 2015). The temptation in the flat-sky case is to approximate $|D_\ell| = \ell^2$, but this is a poor approximation (see section 3.1). The G matrix is given by

$$G_\ell^{SB}(k, \tilde{k}) = \int dz_p j_\ell(kr(z_p)) n(z_p) \times \int dz' p(z'|z_p) U_\ell(r[z'], \tilde{k}), \quad (4)$$

where $n(z_p) dz_p$ is the number of galaxies in a spherical shell of radius z_p and thickness dz_p , and $p(z'|z_p)$ is the probability of a galaxy with photometric redshift z_p having a true redshift z' . The U matrix is given by

$$U_\ell(r[z], k) = \int_0^{r[z]} dr' \frac{F_K(r, r')}{a(r')} j_\ell(kr') P^{1/2}(k, r'), \quad (5)$$

where $P(k, r[z])$ is the matter power spectrum at comoving distance $r[z]$ and radial wavenumber k . The comoving distance r is used to express the time-dependence of the power spectrum; we could equally use t as a label, or $r(t)$. $F_K = S_K(r - r') / S_K(r) / S_K(r')$ is the ‘lensing kernel’ where $S_K(r) = \sinh(r)$, $r, \sin(r)$ for cosmologies with spatial curvature $K = -1, 0, 1$, and $a(r)$ is the dimensionless scale factor at the cosmic time related to the look-back time at comoving distance r . Note that already we have made an approximation, in that the statistics strictly depend on unequal-time

correlators (Kitching & Heavens 2016), but we will not discuss this point further here.

2.2 The Spherical-Radial Representation

A different way to represent the three-dimensional shear field is to make a Fourier-like decomposition in angular wavenumber but *not* in the radial direction. This decomposition is the following

$$\gamma_\ell^m(z) = \sum_{g \in z} \gamma_g(r_g, \theta_g) {}_2Y_\ell^m(\theta_g) \quad (6)$$

which is still a three-dimensional representation of the data, except that it excludes the radial Bessel transform. The sum in this case is over all galaxies that have a redshift z . We refer to this as the ‘spherical-radial’ transform (as opposed to a spherical-Bessel transform).

Again the mean of this representation is zero, but the covariance is non-zero. Using the notation above, we can write down the theoretical expectation value of the power spectrum given a cosmology

$$C_\ell^{SR}(z, z') = |D_\ell|^2 \mathcal{A}^2 \int \frac{dk}{k^2} G_\ell^{SR}(z, k) G_\ell^{SR}(z', k), \quad (7)$$

where in this case the G^{SR} matrix is given by

$$G_\ell^{SR}(z, k) = \int dz_p W^{SR}(z, z_p) n(z_p) \times \int dz' p(z'|z_p) U_\ell(r[z'], k), \quad (8)$$

where $W(z, z_p)$ is a redshift-dependent weight function that defines the ‘bin-width’ in redshift over which the statistic is defined for redshift z . The U matrices are the same as in equation (5). In the case that $W^{SR}(z, z_p) = \delta^D(z - z_p)$ this covariance is still a complete representation of the shear field when z and z' span $[0, \infty)$.

2.3 The Configuration-Space Representation

As an alternative to performing a cosmic shear statistic in Fourier/Bessel space the analysis can be done in real/angular/configuration space, where instead of an angular wavenumber an angle θ is used on the celestial sphere as the dependent variable. Such statistics are readily computed from data by summing over pairs of galaxies (see e.g. Kilbinger, 2015). From theory these are related to the cosmic shear power spectra through a transform that results in two correlation functions

$$\begin{aligned} \xi_+(\theta, z, z') &= \frac{1}{2\pi} \sum_\ell (\ell + 0.5) d_{22}^\ell(\theta) \\ &\quad [C_\ell^{SR,E}(z, z') + C_\ell^{SR,B}(z, z')] \\ \xi_-(\theta, z, z') &= \frac{1}{2\pi} \sum_\ell (\ell + 0.5) d_{-22}^\ell(\theta) \\ &\quad [C_\ell^{SR,E}(z, z') - C_\ell^{SR,B}(z, z')]. \end{aligned} \quad (9)$$

where d_{22}^ℓ and d_{-22}^ℓ are Wigner small- d matrices³. θ are angular separations on the sphere. This can be derived in a number of ways either starting from Hu (2000, Appendix A), from the results of Ng & Liu (1999), or from considering the additive properties of the Wigner large- D matrices. In this case the power spectra in the integrals are a combinations of both E-mode and B-mode components; however from theory the B-mode is typically always zero.

2.3.1 Large Wavenumber Limit

In the limit that $\ell \gg |m|, |m'|$ (in the cosmic shear case $|\ell| \gg 2$) the Wigner-d matrices can be written as Bessel functions of the first kind, which is what has been done in cosmic shear studies to date. Making the further approximation that $\ell \simeq \ell + 0.5$ the transforms in equation (9) are commonly assumed to be Hankel transforms:

$$\begin{aligned} \xi_+(\theta, z, z') &= \frac{1}{2\pi} \sum_\ell \ell J_0(\ell\theta) \\ &\quad [C_\ell^{SR,E}(z, z') + C_\ell^{SR,B}(z, z')] \\ \xi_-(\theta, z, z') &= \frac{1}{2\pi} \sum_\ell \ell J_4(\ell\theta) \\ &\quad [C_\ell^{SR,E}(z, z') - C_\ell^{SR,B}(z, z')]. \end{aligned} \quad (10)$$

Hankel transforms can be performed using either a three-dimensional power spectrum, as we have used here, or on tomographically binned data. An inverse-Hankel transform can also be defined e.g., $C_\ell^{SR}(z, z') = \int d\theta \theta J_0(\ell\theta) \xi_+(\theta, z, z')$ but since this formally requires an integration over *all* angles it is not well-defined in a flat-sky case.

In the cosmic shear representations that are based on spherical harmonic transforms the angular wavenumbers can be approximately related to celestial angular separations through $\theta = \pi/\ell$. However after performing the Hankel transformation the relationship between the angle θ in equations (10) is more complicated. To investigate this relation we plot in Figure 1 the Bessel function amplitudes in equation (10) as a function of ℓ -mode and θ , for the ξ_+ and ξ_- functions. It is clear from these figures that every angle samples from all ℓ -modes but weighted in a different way. To estimate which ℓ -modes contribute to the Hankel transform integrals we compute the following integrals over θ

$$\begin{aligned} \mathcal{W}_+(\ell, z, z') &= \int_{\theta_{\min}}^{\theta_{\max}} d\theta [\ell J_0(\ell\theta) C_\ell^{SR}(z, z')] \\ \mathcal{W}_-(\ell, z, z') &= \int_{\theta_{\min}}^{\theta_{\max}} d\theta [\ell J_4(\ell\theta) C_\ell^{SR}(z, z')]. \end{aligned} \quad (11)$$

These are the weight functions in ℓ -mode, integrated over all angles, that are applicable for analyses that require a sum over angle (such as a likelihood function). We use $\theta_{\max} = 100$ arcminutes, and vary θ_{\min} and show these functions in Figure 1. To compute the maximum ℓ -mode to minimum θ relationship we compute the cumulative functions

$$\left(\frac{1}{A}\right) \int_2^{\ell_{\max}} d\ell |\mathcal{W}_+(\ell, r, r')| = f \leq 1, \quad (12)$$

³ We provide tabulated values of these here <http://goo.gl/UUQIUx>.

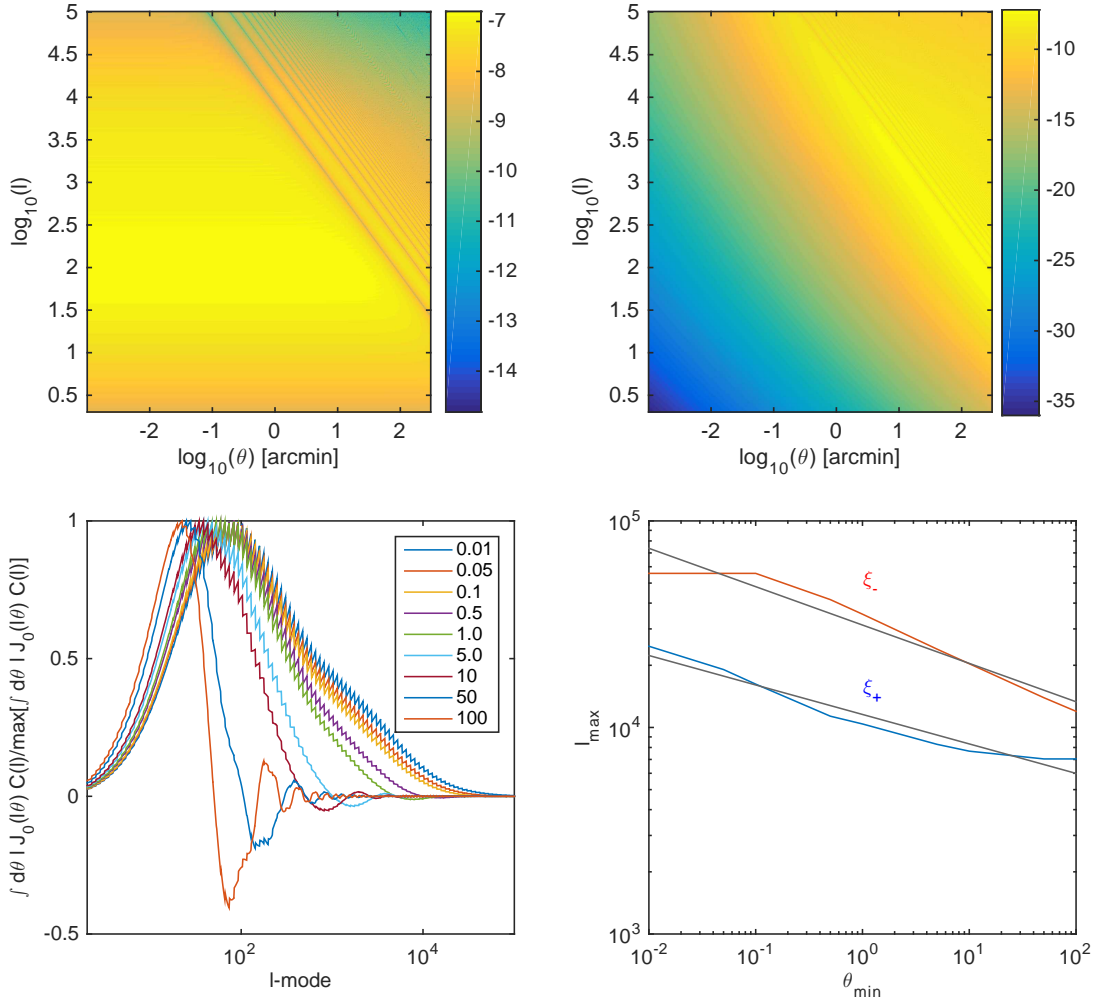


Figure 1. The top panels show the functions $\ell J_0(\ell\theta)C_\ell^{SR}(z, z)$ (left-hand panel) and $\ell J_4(\ell\theta)C_\ell^{SR}(z, z)$ (right-hand panel) for an auto-correlation cosmic shear power spectrum $C_\ell^{SR}(z, z)$ evaluated at a redshift of zero; although we find results in this Figure are insensitive to this assumption. The colour scales denote the logarithm (base-10) of the magnitude of the functions that correspond to the ξ_+ and ξ_- Hankel transforms (equation 10) respectively. The lower left panel shows the normalised integral $\int d\theta \ell J_0(\ell\theta)C_\ell^{SR}(z, z)$ over θ to show the integrated weighting of $\int d\theta \xi_\pm(\theta)$ as a function of ℓ -modes for a variety of angular ranges $\theta_{\min} \leq \theta/\text{arcmin} \leq 100$. The different labelled colours in this plot show different θ_{\min} in arcminutes. The lower right-hand panel shows the ℓ_{\max} where these integrals converge as a function of θ_{\min} for the ξ_+ (blue) and ξ_- (red) Hankel transforms. The fitted functions in equation (13) are shown in grey.

that we calculate as a discrete sum, where $A = \int_2^\infty d\ell |\mathcal{W}_+(\ell, r, r')|$. These functions only converge to machine precision at $\ell_{\max} \rightarrow \infty$ so in practice a tolerance needs to be defined f where it is considered that most of the information is captured. We set this to $f = 0.995$, i.e. 99.5% of the integral content is captured by this limit; we find that setting a limit larger than this results in numerical errors becoming dominant. We plot this derived ℓ_{\max} in Figure 1, and find that the link between ℓ_{\max} and θ_{\min} is well-approximated by the following scaling functions

$$\begin{aligned} \xi_+ : \log_{10}[\ell_{\max}] &= -0.14 \log_{10}(\theta_{\min}/\text{arcmin}) + 4.06 \\ \xi_- : \log_{10}[\ell_{\max}] &= -0.19 \log_{10}(\theta_{\min}/\text{arcmin}) + 4.49. \end{aligned} \quad (13)$$

We find that the ξ_- statistic is much more sensitive to high- ℓ modes than ξ_+ . For typical minimum angles used in data analysis of $\theta_{\min} \sim 0.1$ arcminutes we find that the maximum

wavenumber probed is approximately $\ell_{\max} \sim 5 \times 10^4$ for the ξ_+ statistic, but the bulk of the signal comes from $\ell < 1000$.

To estimate correlation functions from data formally requires summing over all galaxy pairs separated by arbitrary angles from zero separation to infinity (Kilbinger, 2015). In practice such a sum is not possible, therefore several ways of filtering the ‘raw’ correlation function measurement (equation 10) have been proposed that result in finite angular limits, for example Top-hat statistics, Map statistics (e.g. Munshi et al., 2004) and COSEBIs (e.g. Schneider et al., 2010). These are well summarised and reviewed in Kilbinger (2015).

3 COSMIC SHEAR APPROXIMATIONS

We will now investigate the impact of several approximations that are commonly used in cosmic shear stud-

ies. We will address the flat-sky and Limber approximations, but will not discuss source-source clustering (Schneider et al. 2002), source-lens clustering (Bernardeau 1998, Hamana et al. 2002), the Born approximation (Cooray & Hu, 2002), higher-order power spectrum terms (Krause & Hirata, 2010), or unequal-time correlators (Kitching & Heavens, 2016); all of which are expected to have an effect for future surveys (Euclid, LSST and WFIRST) but not for current surveys.

3.1 The Flat-Sky Approximation

The flat-sky approximation assumes that the angular extent of the observational field is small and hence the geometry of the angular component is assumed to be planar (i.e., Euclidean). In this case a planar transform is done instead of a spherical transform in equations (1) and (6) which results in an exponential term $\exp(i\ell\theta)$ instead of the spin spherical harmonics.

In the case of computing the transform coefficients from data, equations (1) and (6), this results in a different sum over galaxies. In the computation of data vectors the weighting as a function of ℓ mode is therefore significantly different (see e.g. Hu, 2000).

However in the computation of the theoretical covariances, due to the similar orthogonality relations between both the spherical harmonic and the exponential functions, equations (3) and (7), this only results in a simple change to the pre-factor $|D_\ell|$ from $|D_\ell| = \sqrt{(\ell+2)!/(\ell-2)!} \rightarrow \ell^2$. This is a result of the different ways that the spin raising and lowering operators (that relate the shear field to the gravitational potential field) act on the spin spherical harmonics and the exponential functions; see Appendix A of Castro et al. (2005). The impact of this approximation on the amplitude of the cosmic shear covariance can then very simply be computed.

We note that taking a small angle approximation of the spherical harmonics (see Castro et al., 2005 Section V; or Varshalovich, Moskalev, & Khersonskii, 1988 for more complete expressions) results in much larger differences in the amplitude of the power spectra than that captured in the change of local derivative of the lens potential, but this case has not been considered in the cosmic shear literature to date.

3.2 Tomographic Data Compression

The tomographic approximation involves the computation of projected two-dimensional power spectra in a series of redshift bins including the inter-bin (auto-correlation) and intra-bin (cross-correlation) power spectra. This is not an approximation in itself, but it is a lossy data compression.

We look at the effect of this binning by first relating the spherical-Bessel and spherical-radial transforms together. As shown in Kitching et al. (2014) the shear transform coefficients, from our equations (1) and (6), can be related through a radial transform

$$\gamma_\ell^m(z_1) = \int dr W^{SR}[z_1, z(r)] \int dk j_\ell(kr) \gamma_\ell^m(k) \quad (14)$$

where the weight function is the same one that appears in

equation (8), where the integrand of comoving distance r is related to a redshift $z(r)$, and describes the bins as a function of redshift. When referring to tomography we use numbered redshifts e.g. z_1 and z_2 , rather than z and z' . We note that only in the case that the weight function is a delta-function is this a full description of the three-dimensional shear field. In the case that the bin-width is finite we will refer to this as a ‘tomographic’ representation of the shear field.

By taking the covariance of equation (14) the two power spectra can be related through

$$C_\ell^{SR}(z_1, z_2) = \int dk dk' dr' dr'' W^{SR}[z_1, z(r')] W^{SR}[z_2, z(r'')] j_\ell(kr') j_\ell(k'r'') C_\ell^{SB}(k, k'). \quad (15)$$

This transformation from spherical-Bessel to spherical-radial (tomographic) representations can be performed for any integrable weight function W^{SR} ; this is also discussed in Castro et al. (2005).

The reverse transform can also be computed, but *only* in the case that the weight function is a delta-function in redshift. In this specific case the reverse transform is

$$C_\ell^{SB}(k, k') = \int dz dz' j_\ell(kr[z]) j_\ell(k'r[z']) C_\ell^{SR}(z_1, z_2), \quad (16)$$

where the integration over redshift is formally over $0 \leq z < \infty$.

It has been shown (e.g. Bridle & King, 2007) that only 10 – 20 redshift bins are required in order for the cosmic shear power spectrum to be sufficiently sampled in redshift to extract the majority of cosmological information. This is because the lensing kernel is a relatively broad function in redshift space. This is applicable when describing the shear field using the spherical-radial representation, with the caveats that such current studies of the convergence of this approximation have assumed the flat-sky and Limber approximations (that we discuss in the next Section).

3.3 The Limber Approximation

The Limber (Limber, 1953) approximation was first introduced in Kaiser (1998) for cosmic shear studies as a method for rendering the calculations more tractable and understandable, and has subsequently been used in the majority of the cosmic shear studies, both in methodological development and in applications to data. In LoVerde & Afshordi (2008) a particularly clear explanation of the approximation was provided. This assumed that the matter power spectrum was not evolving, i.e. it can be expressed as a function of k -mode only $P(k)$ (LoVerde & Afshordi, 2008; equation 5). Unfortunately the LoVerde & Afshordi (2008) approximation is not directly appropriate at all orders for the cosmic shear setting where the shear field is an integrated effect over an evolving matter power spectrum; an assumption that we address in Appendix A. In Kitching, Heavens, Miller (2011) the effect of the Limber approximation on cosmic shear was investigated using the LoVerde & Afshordi (2008) approximation, and an effect on the expected error bars of cosmological parameters was predicted.

If the Limber approximation is assumed then using the

Kaiser (1998) and LoVerde & Afshordi (2008) approximation the spherical-radial representation of the cosmic shear field can be written as

$$C_\ell^{SR}(z_1, z_2) \simeq |D_\ell|^2 \mathcal{A}^2 \int \frac{dk}{k^2} P(k, \nu/k) f(z_1, \nu/k) f(z_2, \nu/k) \quad (17)$$

where the variable $\nu = \ell + 1/2$. In Appendix A we show that this is indeed the first order approximation to the cosmic shear power spectrum despite the assumption of a constant matter power spectrum, however the expansion of this to higher order results in a convergence towards the unapproximated case only if redshift-independent limits in angular wavenumber are assumed. The kernel functions are

$$f(z_1, \nu/k) = \frac{\left(\frac{\pi}{2\nu k^2}\right) \int dz' dz_p n(z_p) p(z'|z_p) W^{SR}(z_1, z_p) F_K(r[z'], \nu/k)}{a(\nu/k)}. \quad (18)$$

This expression is not entirely in the same form as commonly used in the cosmic shear literature (e.g. Hu, 1999; Joachimi & Bridle, 2009; Heymans et al. 2013), where the standard form is to use an inner integral over r instead of k -mode. As shown in Appendix A when doing this we find that the Limber-approximated power is given by

$$C_\ell^{SR}(z_1, z_2) \simeq D_\ell^2 \mathcal{A}^2 \left(\frac{1}{\nu^4}\right) \int dr q(r_1, r) q(r_2, r) P(\nu/r, r), \quad (19)$$

where

$$q(r_1, r) = \frac{r}{a(r)} \int dz_p dz'_p n(z_p) p(z|z_p) W^{SR}(z_1, z_p) \left(\frac{r(z') - r}{r'}\right) \quad (20)$$

where we have expanded the function F_K , and we have assumed here a flat-geometry ($K = 0$). This is the standard form for the cosmic shear power spectrum (see e.g. Hu, 1999; Joachimi & Bridle, 2009), except that there is an ℓ -dependent pre-factor

$$T_\ell = \frac{D_\ell^2}{\nu^4} = \frac{(\ell + 2)(\ell + 1)\ell(\ell - 1)}{(\ell + 0.5)^4}. \quad (21)$$

T_ℓ is normally replaced by 1. One justification for this is to replace the numerator by ℓ^4 in the flat-sky approximation, and to take a high- ℓ approximation $\nu \simeq \ell$ in the denominator. Note that a flat-sky approximation that also retains the Limber ν^{-4} dependence would lead to an inaccurate T_ℓ which differs from unity at $\mathcal{O}(1/\ell)$, and leads to significant errors at low ℓ . Note that T_ℓ differs from unity only at $\mathcal{O}(1/\ell^2)$, so the standard approximation is good for current data, but there is no reason at all not to use the full expression.

Up to first order the Limber approximation can be summarised by comparing equation (7) with equation (17) as a replacement of Bessel functions with scaled delta functions inside the integrals

$$j_\ell(kr) \rightarrow \sqrt{\frac{\pi}{2\ell + 1}} \delta^D(\ell + 1/2 - kr). \quad (22)$$

This expression shows how the Limber approximation acts to link the angular and radial modes through the relation $\ell = kr[z] - 1/2$, that we also derive in Appendix A, which

has an important effect on the computation of cosmic shear power spectra.

3.4 The Impact of the Approximations

There are various steps in the derivation of a configuration-space shear statistic, which involve relating the lensing potential power spectrum on the (spherical) sky to the matter power spectrum, then computing the shear power spectrum on the sky, and from there transforming to configuration space if desired. These steps can introduce approximations beyond the Born approximation and approximations of unequal time correlators, but some are not necessary. At the first stage, it may be necessary to use the Limber approximation for computational tractability reasons. At low ℓ this is a poor approximation, and if speed is an issue, the next term in the Limber approximation (LoVerde & Afshordi 2008) should be considered. In moving from lensing potential to shear, the full ℓ -dependent prefactor of $(\ell + 2)(\ell + 1)\ell(\ell - 1)$ should be included, and not approximated by the flat-sky ℓ^4 value. If the Limber approximation is used, $\ell + 1/2$ should not be approximated by ℓ . Finally, in computing configuration-space quantities such as shear correlation functions, finite sums over ℓ should be done, using Wigner small-d matrices (equation 9), and not approximated by Hankel transforms.

In summary in going from the full cosmic shear expressions to those that are commonly used there are a series of approximations. These are, starting from a spherical-sky non-Limber-approximated power spectrum:

- **Flat-Sky Approximation:** The assumption of a flat-sky changes the pre-factor in the shear-shear power spectrum from $(\ell + 2)(\ell + 1)\ell(\ell - 1)$ to ℓ^4 . This is inaccurate and unnecessary.
- **Limber Approximation:** The first-order Limber approximation involves changing the Bessel functions to scaled delta functions using equation (22), leading to a prefactor in the shear power spectrum of $(\ell + 2)(\ell + 1)\ell(\ell - 1)/(\ell + 0.5)^4$.
- **Prefactor Unity Approximation:** In the Limber function expression a further approximation can be made that the ℓ -dependent pre-factor is unity i.e. $T_\ell = 1$ in equation (21). This is good to $\mathcal{O}(1/\ell^2)$, but is unnecessary.
- **Integral Variable Approximation:** In the Limber approximation the inner variable $\ell + 0.5$ is sometimes replaced by ℓ in the argument to the matter power spectrum. This is inaccurate and unnecessary.
- **Hankel Transform Approximation:** Then when transforming to real-space a Hankel transform can be used instead of a spherical sky correlation function (equation 9). This leads to an increasing error with angle, and a spherical summation over ℓ modes is preferred.

Each of these approximations act independently, the first four act on the cosmic shear power spectrum, and the last only in the case that this is transformed to real-space.

3.4.1 Impact on the Power Spectrum

In Figure 2 we show the impact of the Flat-Sky, Limber and Prefactor-Unity approximations. Throughout we do not make the Integral Variable Approximation. It can be seen that for $\ell \lesssim 10$ there is a more than 10% suppression in the

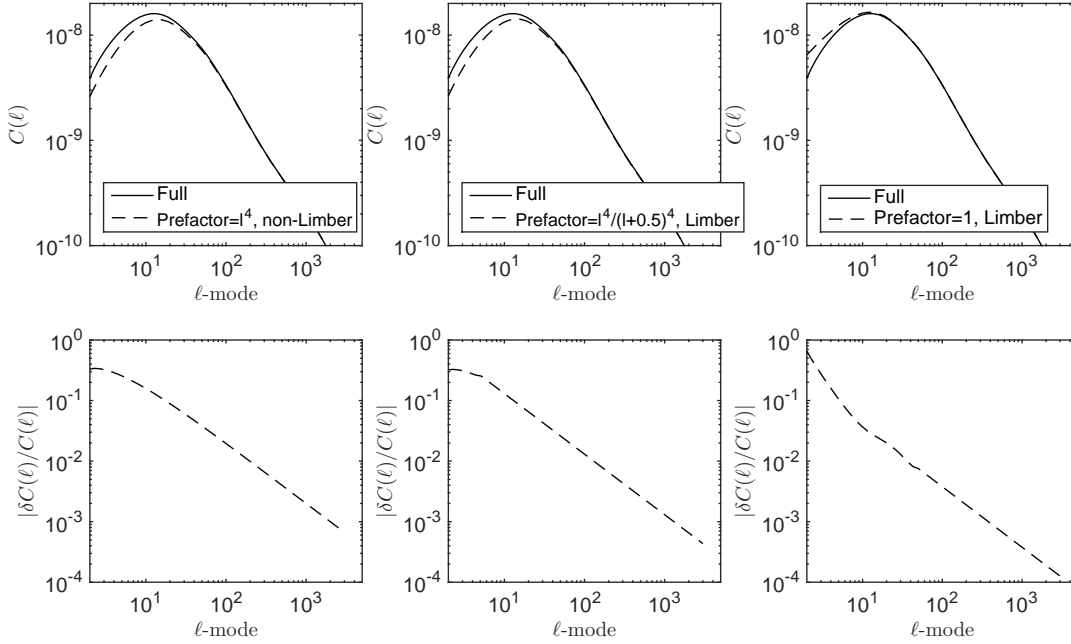


Figure 2. Top panels: The solid line is the full $C(\ell)$ cosmic shear power spectrum, for a CFHTLenS $n(z)$; not assuming any of the approximations listed in Section 3.4 i.e. flat-sky, Limber, prefactor-unity or integral variable assumptions. In the full case the ℓ -dependent prefactor to the power spectrum is $(\ell + 2)!/(\ell - 2)!$ and the Limber approximation is not assumed. The dashed lines show the power spectrum when each of the approximations is applied in combination in the panels from left to right, the ℓ expressions denote the power spectrum pre-factor used. The lower panels show the modulus of the fractional difference between the full case and the approximated cases $||C^{\text{Full}}(\ell) - C^{\text{Approx}}(\ell)||/C^{\text{Full}}(\ell)$.

power due to the Flat-Sky Approximation which reduces to $\lesssim 1\%$ for $\ell \gtrsim 100$. We can assess the impact of these approximations by computing the integrated effect over the differences

$$\langle \mathcal{A} \rangle / N_A = \frac{\int d \ln \ell \ell^2 \delta C(\ell)}{\int d \ln \ell \ell^2} \quad (23)$$

complementary formulations are provided for this quantity in Massey et al. (2013), Cropper et al. (2013) and Amara & Refregier (2008); here we include a normalisation $N_A = \int d \ln \ell \ell^2$ as suggested by Massey et al. (2013). In general a non-zero $\langle \mathcal{A} \rangle$ will change the amplitude of the power spectrum and bias cosmological parameter inference. As discussed in Massey et al. (2013) the requirement on the amplitude of this quantity is $\langle \mathcal{A} \rangle / N_A \leq 1.8 \times 10^{-12}$ for a Euclid- or LSST-like weak lensing survey to return unbiased results on the dark energy equation of state parameters, this requirement is an allowance for *all* systematic effects including instrumental and algorithmic quantities. We find that for best approximated case to the full power spectrum (where the prefactor is unity and the Limber approximation is assumed) that $\langle \mathcal{A} \rangle / N_A = 1.9 \times 10^{-13}$, that would account for 11% of the total budget for systematic effects for a Euclid or LSST-like experiment that suggests such approximations should not be used. If scales of $\ell < 100$ are ignored then we find only a modest change with $\langle \mathcal{A} \rangle / N_A = 1.7 \times 10^{-13}$ (note the ℓ^2 factor in equation 23 that gives higher weight to larger ℓ -modes).

3.4.2 Impact on the Correlation Functions

In Figure 3 and 4 we show the impact of the successive approximations on the real-space correlation functions.

Similarly to the power spectrum investigations we find that the Flat-sky approximation on its own has a large effect, but that again the assumption of a unity prefactor cancels out the approximation changes somewhat. In general we find that these low- ℓ approximations have a more significant impact on ξ_+ than ξ_- , as may be expected from Section 2.3. The additional step of assuming a Hankel transform rather than a transform that uses Wigner small-d matrices (equation 10 instead of equation 9) results in only a small additional change at scales greater than 10 arcminutes; we show only this effect in Figure 5.

There are currently no explicit requirements set on the correlation function amplitude changes in the literature for future experiments that we are aware of, so it is not possible to assess the applicability of these requirements for *Euclid*-like experiments. However we note that percent to tens of percent-level changes can occur and, given that the full case is not particularly more computationally demanding than the approximate cases, we recommend that the full case is used.

3.5 A Schema of Cosmic Shear Statistics

Each of the cosmic shear representations and approximations can be linked in a series of transformations that relate one to the other. For example in Kitching, Heavens, Miller

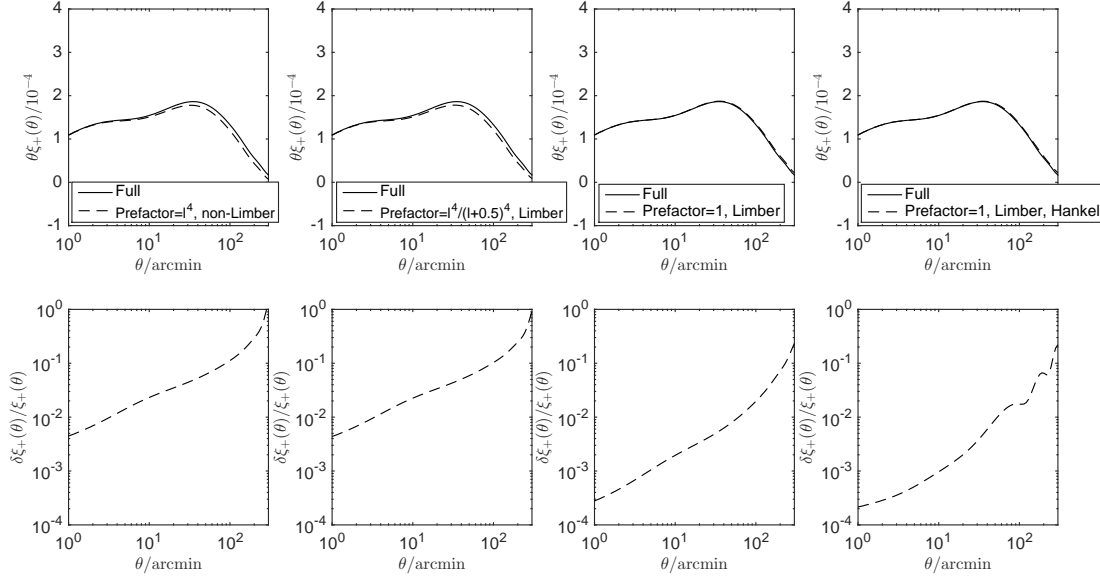


Figure 3. Top panels: The solid line is the full projected $\xi_+(\theta)$ cosmic shear correlation function, for a CFHTLenS $n(z)$; not assuming any of the approximations listed in Section 3.4 i.e. flat-sky, Limber, prefactor-unity, integral variable, or Hankel assumptions. In the full case the ℓ -dependent prefactor to the power spectrum is $(\ell + 2)!/(\ell - 2)!$, the Limber approximation is not assumed, and a transform using Wigner small-d matrices (equation 9) is used. The dashed lines show the correlation function when each of the approximations is applied in combination in the panels from left to right. The lower panels show the modulus of the fractional different between the full case and the approximated cases $|\xi_+^{\text{Full}}(\theta) - \xi_+^{\text{Approx}}(\theta)|/\xi_+^{\text{Full}}(\theta)$.

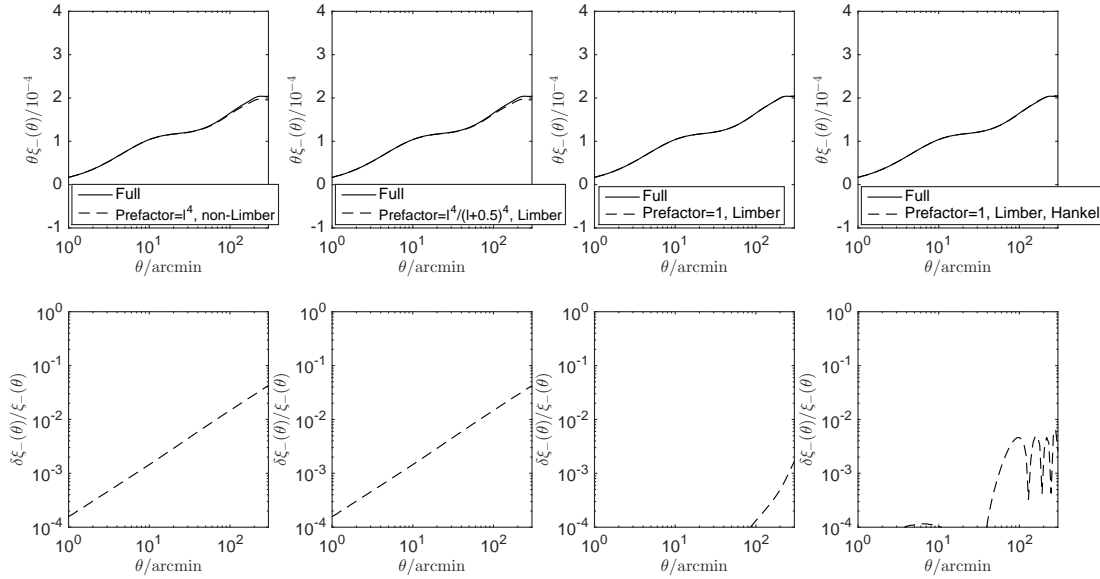


Figure 4. Top panels: The solid line is the full projected $\xi_-(\theta)$ cosmic shear correlation function, for a CFHTLenS $n(z)$; not assuming any of the approximations listed in Section 3.4 i.e. flat-sky, Limber, prefactor-unity, integral variable, or Hankel assumptions. In the full case the ℓ -dependent prefactor to the power spectrum is $(\ell + 2)!/(\ell - 2)!$, the Limber approximation is not assumed, and a transform using Wigner small-d matrices (equation 9) is used. The dashed lines show the correlation function when each of the approximations is applied in combination in the panels from left to right. The lower panels show the modulus of the fractional different between the full case and the approximated cases $|\xi_-^{\text{Full}}(\theta) - \xi_-^{\text{Approx}}(\theta)|/\xi_-^{\text{Full}}(\theta)$.

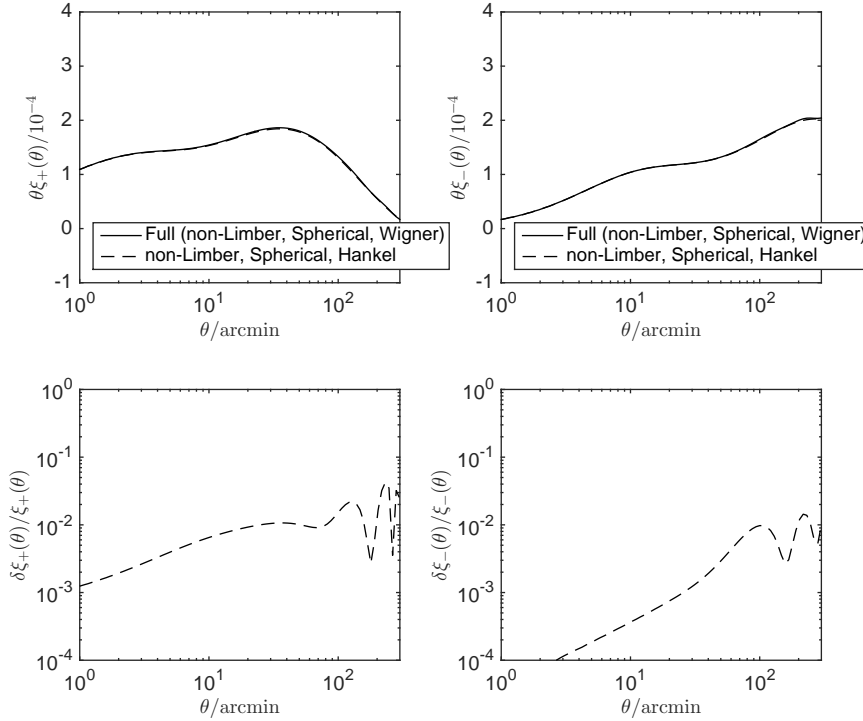


Figure 5. Top panels: The solid line is the full projected $\xi_{+/-}(\theta)$ cosmic shear correlation function, for a CFHTLenS $n(z)$; not assuming any of the approximations listed in Section 3.4 i.e. flat-sky, Limber, prefactor-unity, integral variable, or Hankel assumptions. The dashed lines show the power spectrum when the Hankel transform instead of the full Wigner-d expression is used. The lower panels show the modulus of the fractional different between the full case and the approximated cases.

(2011) and Kitching et al. (2014) we show how to relate the spherical-Bessel to the tomographic representation (we also show this in Appendix A). In this paper we show how to transform from the spherical-Bessel to spherical-radial cases. The flat-sky and configuration-space approximations are well-known as we have discussed.

We show how all of these are linked together in Figure 4 where we relate each of the cosmic shear statistics together via the network of approximations that can be employed. In this Figure arrows indicate the direction that the transform takes the statistic, where only one such case is reversible⁴ (the three-dimensional radial transform). We also link the points at which estimators from data are linked to the theoretical statistics, and highlight those statistics that have been applied to data. This provides a visual way to understand what transformation need to be made to interpret any given cosmic shear data analysis, where any statistical assumptions have been made, and how a given observation can be translated into another.

4 DISCUSSION

There have been several other investigations into the Limber approximation. For example Giannantonio et al., (2012) con-

cluded that the Limber approximation is accurate for $\ell \gtrsim 20$. However Giannantonio et al. (2012, equations 25 and 26) are not in detail applicable for cosmic shear: they neglect a factor of $(\ell + 2)!/(\ell - 2)!$ (or l^4 in the flat sky limit), and also use k^2 in the inner integral (β in their notation) not $(1/k^2)$ (which is the appropriate factor for the cosmic shear case). Therefore the Giannantonio et al. (2012) result is effectively for a weighted galaxy-clustering-projected $C(\ell)$.

Jeong et al. (2009) tested the effect of the Limber approximation on the convergence-convergence power spectra and found a $\sim 1\%$ change in power at $\ell \lesssim 100$, and a 10% change at scales $\ell \lesssim 10$. This result is partly consistent with our analysis where a 10% change in the amplitude of the $C_\ell^{SR}(z, z')$ shear-shear power spectrum at $\ell \sim 10$ would propagate into ξ_+ and ξ_- statistics with a similar decrease in power on the real-space angular scales presented in current data analyses. However the range of k -modes and redshift ranges is not quoted in that paper (in particular if a $kr < \ell$ limit is imposed or not) which makes a detailed comparison difficult. Simon (2007) performed a similar study of the Limber approximation in the galaxy clustering context and found that there is a $\sim 10\%$ bias in the correlation function at scales of $\theta \simeq 260$ arcminutes.

Bernardeau et al. (2012) show that the Limber-approximated power spectrum is accurate to better than 1% at $\ell > 8$, however they also look at the projected galaxy power spectrum rather than the cosmic shear case. This can be seen in their equations (e.g. 44) where a factor k^2 de-

⁴ By reversible we mean that it can be performed in either direction, without loss of information.

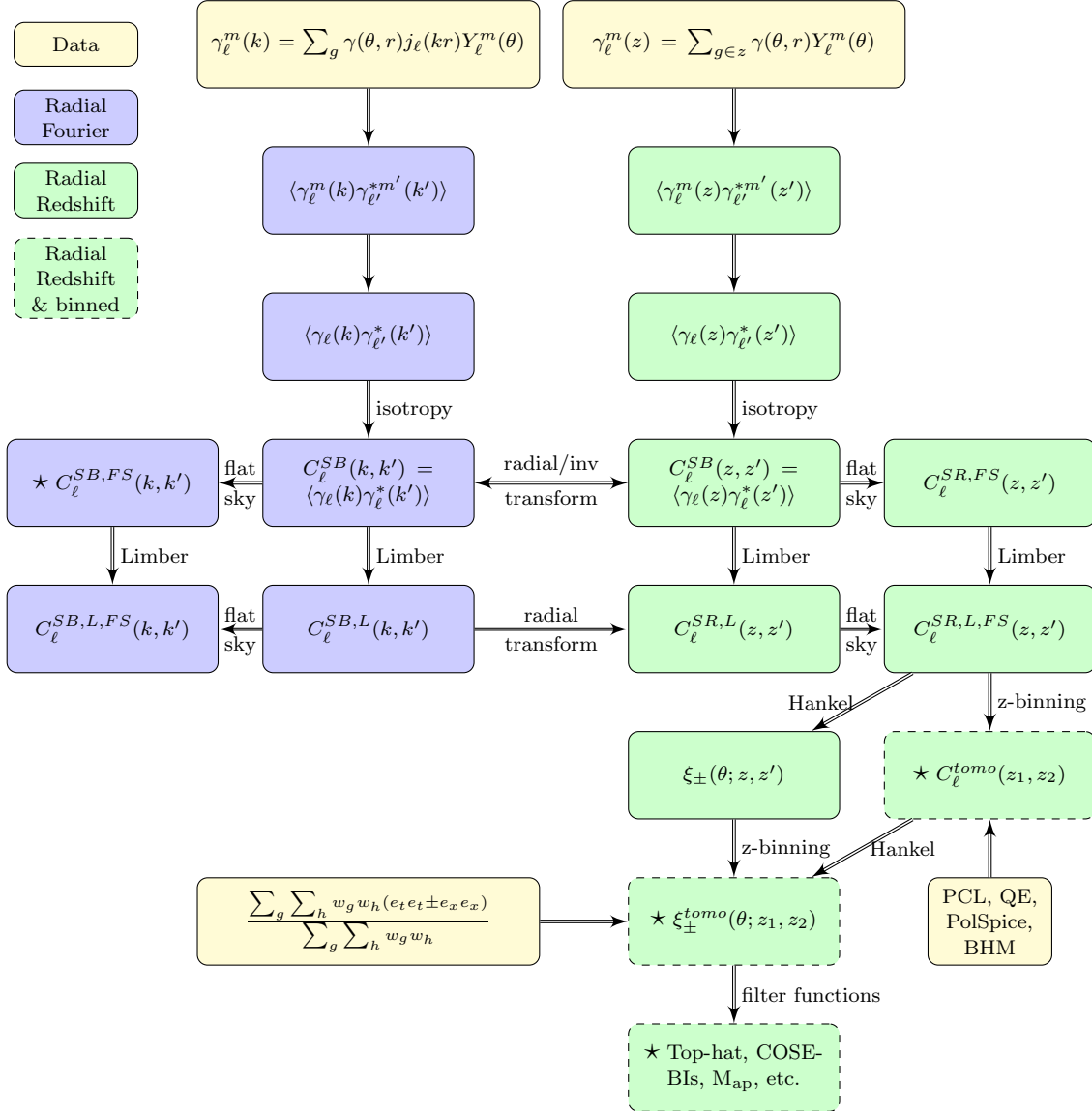


Figure 6. A schema relating each cosmic shear approximation to all others. For brevity we do not include spherical-sky, or non-Limber-approximated Hankel-like transforms (defined in Castro et al., 2005, Section V) as these are not currently in use. Each arrow shows the direction in which a functional approximation or change is applied where the majority of approximations are irreversible. The yellow boxes show places where a statistic can, and has, been approximated from data; these are a direct spherical-Bessel transform (top), a direct correlation function estimator (left), and several power spectrum estimators that are Pseudo- $C(\ell)$ (e.g. Hikage et al., 2011), Quadratic Estimator (Hu & White, 2001), PolSpice (The DES Collaboration et al., 2015) and Bayesian Hierarchical Modelling (BHM, e.g. Alsing et al., 2016a,b, Schneider et al., 2016a,b). The blue boxes show statistics that treat the radial (redshift) direction using a Fourier-like/spherical-Bessel analysis, the green boxes show statistics that treat the radial direction directly in redshift space. The solid framed boxes denote full three-dimensional statistics and the dashed framed boxes show redshift binned or ‘tomographic’ statistics. The superscript acronyms SB, SR, FS and L refer to spherical-Bessel, spherical-radial, flat-sky and Limber approximations respectively. Isotropy refers to angular isotropy but not radial, as the shear field probes different look-back times in the expansion history. The labels (k, k') and (z, z') denote continuous scale and redshift variables, and (z_1, z_2) to discretised redshifts. The lower box denoting filter functions refers to Map (e.g. Munshi et al., 2004), COSEBI (Schneider et al. 2010) and top-hat statistics. The stars \star show which statistics have been applied to data.

notes that the power spectrum rather than the Newtonian potential is being probed (which would have a denominator of k^2), similar to Giannantonio et al. (2012).

Kitching et al. (2011) applied the LoVerde & Afshordi (2008) approximation (equation 22) in the spherical-Bessel case and compared the case of full (k, z) integration with the $\ell > kr$ case, and found a $< 10\%$ change in the amplitude

of $C_{\ell}^{\text{SB}}(k, k')$ using the Limber approximation which was approximately constant as a function of ℓ -mode, which is consistent with the results found in this paper. Including the first and second order corrections suggested by LoVerde & Afshordi (2008) are likely to reduce the impact further at low ℓ -modes.

Power spectrum methods, that measure the cosmic

shear two-point statistics as a function of ℓ -mode, are more immune to these approximations than correlation function methods because removing $\ell \lesssim 100$ from an analysis will eliminate most of the low- ℓ mode effects. This is the approach taken in Köhlinger et al. (2015) and Alsing et al. (2016b) (both of which made the flat-sky, Limber and tomographic approximations). However power spectrum methods that use a pseudo- $C(\ell)$, or a mixing matrix method, to account for real-space masks will also encounter additional complexity if the masks mix low- ℓ modes and higher ℓ -modes (e.g. Hikage et al., 2011). Finally super-sample covariance (Takada & Hu, 2013) that causes correlations between the power spectrum errors across ℓ -modes that will also mix low- ℓ and high- ℓ behaviour.

5 CONCLUSION

In this paper we present the spherical-Bessel and spherical-radial representations of cosmic shear, and discuss the correlation function representation. We discuss several approximations and limits of these statistics including the flat-sky, tomographic and Limber approximations. Whilst the tomographic approximation is expected to be relatively benign – because the lensing kernel is relatively smooth in redshift – the flat-sky and Limber approximations change the statistical behaviour of the cosmic shear statistic at large-scales. We also find a subtlety in the derivation of the standard Limber-approximated cosmic shear power spectra formula that neglects an ℓ -dependent factor of

$$T_\ell = \frac{(\ell + 2)(\ell + 1)\ell(\ell - 1)}{(\ell + 0.5)^4}, \quad (24)$$

which is equal to unity if the flat-sky approximation is used, and the factor of 0.5 in the denominator is ignored. To include this effect any cosmic shear potential power spectrum $C(\ell)$ (Limber-approximated or not) should be multiplied by this factor.

We investigate how the angular scales in correlation function analyses map onto ℓ -modes of the cosmic shear power spectrum and find that the following scaling relations are a good fit to the behaviour

$$\begin{aligned} \xi_+ : \log_{10}[\ell_{\max}] &= -0.14 \log_{10}(\theta_{\min}/\text{arcmin}) + 4.06 \\ \xi_- : \log_{10}[\ell_{\max}] &= -0.19 \log_{10}(\theta_{\min}/\text{arcmin}) + 4.49. \end{aligned} \quad (25)$$

We also present mapping between the various cosmic shear statistics used in the literature. In translating from the shear power spectrum to configuration statistics such as shear correlation functions, the Hankel transform introduces errors on arcminute scales and higher. A full summation over spherical harmonic modes, using Wigner small-d matrices, is straightforward and preferable.

Many of the approximations we have discussed have relatively small effects, but are unnecessary and there is no good reason to apply them, and for future experiments, such as Euclid, LSST and WFIRST, which will have very small statistical errors, they should not be applied. Only the Limber approximation may be necessary, and only if computational speed is an issue, and in this case the inaccuracies at low ℓ may be reduced by considering the first two terms in the Limber expansion in LoVerde & Afshordi (2008).

In this paper we addressed the most prominent approximations, however there are several further approximations that are expected to have additional impacts on cosmological inference such as source-source clustering (Schneider et al. 2002), source-lens clustering (Bernardeau 1998, Hamana et al. 2002), the Born approximation (Cooray & Hu, 2002), higher-order power spectrum terms (Krause & Hirata, 2010), and the full treatment of unequal-time correlations (Kitching & Heavens, 2016).

Acknowledgements: TDK is supported by Royal Society University Research Fellowship. RJ & LV acknowledge support by Spanish Mineco grant AYA2014-58747-P and MDM-2014-0369 of ICCUB (Unidad de Excelencia ‘Maria de Maeztu’ and Royal Society grant IE140357. JDM is supported in part by the Engineering and Physical Sciences Research Council (grant number EP/M011852/1). The Centre for Computational Astrophysics is supported by the Simons Foundation. We thank the creators of CAMB for public release of this code. We thank M. Cropper, H. Hoekstra, A. Lewis, and P. Paykari for useful and constructive discussions. We thank C. Wallis for providing the Wigner small-d matrices.

REFERENCES

- Albrecht, A., Bernstein, G., Cahn, R., et al. 2006, arXiv:astro-ph/0609591
- Alsing, J., Heavens, A., Jaffe, A. H., et al. 2016, MNRAS, 455, 4452
- Alsing, J., Heavens, A. F., Jaffe, A. H., 2016, arXiv, 1607.00008
- Alsing, J., et al., in prep
- Amara, A., & Réfrégier, A. 2008, MNRAS, 391, 228
- Battye, R. A., Moss, A., & Pearson, J. A. 2015, JCAP, 4, 048
- Bernardeau, F., 1998, A&A, 338, 375
- Bridle, S., & King, L. 2007, New Journal of Physics, 9, 444
- Brown, M. L., Taylor, A. N., Bacon, D. J., et al. 2003, MNRAS, 341, 100
- Castro, P. G., Heavens, A. F., & Kitching, T. D. 2005, PRD, 72, 023516
- Choi, A; et al.; 2016, MNRAS, 463, 2
- Cooray, A., & Hu, W. 2002, Astro. Phys. Journal, 574, 19
- Cropper, M., Hoekstra, H., Kitching, T., et al. 2013, MNRAS, 431, 3103
- Dossett J. N., Ishak M., Parkinson D., Davis T., 2015, ArXiv e-prints
- Fang, W., Hu, W., & Lewis, A. 2008, Phys. Rev. D, 78, 087303
- Fang, W., Wang, S., Hu, W., et al. 2008, Phys. Rev. D, 78, 103509
- Fedeli, C. 2014, JCAP, 4, 028
- Foreman, S., Becker, M. R., & Wechsler, R. H. 2016, arXiv:1605.09056
- Giannantonio, T., Porciani, C., Carron, J., Amara, A., & Pillepich, A. 2012, MNRAS, 422, 2854
- Hamana, T., Colombi, S. T., Thion, A., Devriendt, J. E. G. T., Mellier, Y., et al., 2002, MNRAS, 330, 365
- Harnois-Déraps, J., Vafaei, S., & Van Waerbeke, L. 2012, MNRAS, 426, 1262
- Harnois-Déraps, J., & van Waerbeke, L. 2015, MNRAS, 450, 2857
- Harnois-Déraps, J., Tröster, T., Hojjati, A., et al. 2016, MNRAS, 460, 434
- Heavens, A. F., 2003, MNRAS, 343, 1327
- Heavens, A. F., Kitching, T. D., & Taylor, A. N. 2006, MNRAS, 373, 105
- Heavens, A. F., Kitching, T. D., & Verde, L. 2007, MNRAS, 380, 1029
- Heymans, C., Brown, M. L., Barden, M., et al. 2005, MNRAS, 361, 160
- Heymans, C., Van Waerbeke, L., Miller, L., et al. 2012, MNRAS, 427, 146
- Heymans, C., Grocutt, E., Heavens, A., et al. 2013, MNRAS, 432, 2433
- Hikage, C., Takada, M., Hamana, T., & Spergel, D. 2011, MNRAS, 412, 65
- Hildebrandt, H., Viola, M., Heymans, C., et al. 2016, arXiv:1606.05338
- Hirata, C. M., & Seljak, U. 2004, Phys. Rev. D, 70, 063526
- Hu, W. 1999, Astro. Phys. Journal Letters, 522, L21
- Hu, W. 2000, Phys. Rev. D, 62, 043007
- Hu, W., & Sawicki, I. 2007, Phys. Rev. D, 76, 064004
- Hu, W., & White, M. 2001, Astro. Phys. Journal, 554, 67
- Hoekstra, H., & Jain, B. 2008, Annual Review of Nuclear and Particle Science, 58, 99
- Jeong, D., Komatsu, E., & Jain, B. 2009, Phys. Rev. D, 80, 123527
- Joudaki, S., & Kaplinghat, M. 2012, Phys. Rev. D, 86, 023526
- Kaiser, N. 1998, Astro. Phys. Journal, 498, 26
- Kilbinger, M. 2015, Reports on Progress in Physics, 78, 086901
- Kitching, T. D., Heavens, A. F., Taylor, A. N., et al. 2007, MNRAS, 376, 771
- Kitching, T. D., Taylor, A. N., & Heavens, A. F. 2008, MNRAS, 389, 173
- Kitching, T. D., Heavens, A. F., & Miller, L. 2011, MNRAS, 413, 2923
- Kitching, T. D., Heavens, A. F., Alsing, J., et al. 2014, MNRAS, 442, 1326
- Kitching T. D; Verde, L; Heavens, A.; Jimenez, R.; 2016, MNRAS, doi: 10.1093/mnras/stw707
- Kitching T., & Heavens, A.; 2016, in prep
- Köhlinger, F., Viola, M., Valkenburg, W., et al. 2016, MNRAS, 456, 1508
- Krause, E., & Hirata, C. M. 2010, AAP, 523, A28
- Kuijken, K., Heymans, C., Hildebrandt, H., et al. 2015, MNRAS, 454, 3500
- Laureijs, R., Amiaux, J., Arduini, S., et al. 2011, arXiv:1110.3193
- Leistedt, B., McEwen, J. D., Kitching, T. D., & Peiris, H. V. 2015, Phys. Rev. D, 92, 123010
- Limber, N., 1953, ApJ, 117, 134
- LSST Science Collaboration, Abell, P. A., Allison, J., et al. 2009, arXiv:0912.0201
- Loverde, M., & Afshordi, N. 2008, Phys. Rev. D, 78, 123506
- MacCrann, N., Zuntz, J., Bridle, S., Jain, B., & Becker, M. R. 2014, arXiv:1408.4742
- Mandelbaum, R., Rowe, B., Bosch, J., et al. 2014, ApJS, 212, 5
- Massey, R., Hoekstra, H., Kitching, T., et al. 2013, MNRAS, 429, 661
- Mead, A. J., Peacock, J. A., Heymans, C., Joudaki, S., & Heavens, A. F. 2015, MNRAS, 454, 1958
- Munshi, D., Valageas, P., & Barber, A. J. 2004, MNRAS, 350, 77
- Ng, K.-W., & Liu, G.-C. 1999, International Journal of Modern Physics D, 8, 61
- Pan, Z., Knox, L., & White, M. 2014, MNRAS, 445, 2941
- Pen, U.-L., Van Waerbeke, L., & Mellier, Y. 2002, Astro. Phys. Journal, 567, 31
- Planck Collaboration 2013a, arXiv:1303.5076
- Planck Collaboration, Ade, P. A. R., Aghanim, N., et al. 2015, arXiv:1502.01590
- Planck Collaboration, Ade, P. A. R., Aghanim, N., et al. 2016, AAP, 594, A15
- Sellentin, E.; Heavens, A. F.' 2016, MNRAS, 456, 132
- Schneider, P., Eifler, T., & Krause, E. 2010, AAP, 520, A116
- Schneider, P., Van Waerbeke, L., Mellier, Y. 2002, A&A, 389, 729
- Schneider, M.D., Ng, K.Y., Dawson, W. A., Marshall, P.J., Meyers, J., Bard, D.J., 2016, arXiv:1610.06673
- Semboloni, E., Hoekstra, H., Schaye, J., van Daalen, M. P., & McCarthy, I. G. 2011, MNRAS, 417, 2020
- Simon, P. 2007, AAP, 473, 711
- Smith, R. E., Peacock, J. A., Jenkins, A., et al. 2003, MNRAS, 341, 1311
- Spergel, D., Gehrels, N., Baltay, C., et al. 2015, arXiv:1503.03757
- Takada, M., & Hu, W. 2013, Phys. Rev. D, 87, 123504
- Tegmark, M., Taylor, A. N., & Heavens, A. F. 1997, Astro. Phys. Journal, 480, 22
- The Dark Energy Survey Collaboration, Abbott, T., Abdalla, F. B., et al. 2015, arXiv:1507.05552
- Tröster, T., Camera, S., Fornasa, M., et al. 2016, arXiv:1611.03554
- Varshalovich, D.A. and Moskalev, A.N. and Khersonskii, V.K.; 1988, Quantum Theory of Angular Momentum, World Scientific Pub, ISBN 9789971501075
- van Uitert, E., & Schneider, P. 2016, arXiv:1605.01056

APPENDIX A: THE EXTENDED LIMBER APPROXIMATION FOR COSMIC SHEAR

In LoVerde & Afshordi (2008) an extended Limber approximation is presented that was used to assess the accuracy of this approximation as a function of ℓ -mode. Their main result can be captured in the following approximation

$$\lim_{\epsilon \rightarrow 0} \int_0^\infty e^{-\epsilon(x-\nu)} f(x) J_\nu(x) dx = f(\nu) - \frac{1}{2} f''(\nu) - \frac{\nu}{6} f'''(\nu) + \dots \quad (26)$$

where $\nu = \ell + 1/2$, $J_\nu(x)$ are Bessel functions (not spherical), and $f(x)$ is some arbitrary function. Dashes denote derivatives with respect to x . This is then applied to the case of a non-evolving matter power spectrum $P(k)$ (LoVerde & Afshordi, 2008; equation 5) and an extended Limber approximation computed (LoVerde & Afshordi, 2008; equation 11). This calculation however is not strictly appropriate for the cosmic shear case because the matter power spectrum is an evolving field $P(k, z)$.

For cosmic shear we start with equation (5)

$$U_\ell(r[z], k) = \int_0^{r[z]} dr' \frac{F_K(r, r')}{a(r')} j_\ell(kr') P^{1/2}(k, r'), \quad (27)$$

that describes the kernel function for the spherical-Bessel and spherical-radial representations of the cosmic shear field. The integral is along a line-of-sight to a source redshift plane $r[z]$ and encodes the radial transform of the integrated lensing effect caused by perturbations in the matter over-density, that are mapped to the power spectrum via Poissons equation. To make this into a form for which the LoVerde & Afshordi (2008) expansion can be applied we re-write this as

$$U_\ell(r[z], k) = \int_0^\infty dr' w(r[z], r') \frac{F_K(r, r')}{a(r')} j_\ell(kr') P^{1/2}(k, r'), \quad (28)$$

where $w(r, r')$ is a weight function with the following properties: $w(r, r') = 1$ for $r' \leq r$, and $w(r, r') = 0$ for $r' > r$. We can now apply the Limber approximation and find that to first order

$$U_\ell^L(r[z], k) = \left(\frac{\pi}{2\nu k^2} \right)^{1/2} w(r[z], \nu/k) \frac{F_K(r, \nu/k)}{a(\nu/k)} P^{1/2}(k, \nu/k) + \dots \quad (29)$$

where $\nu = \ell + 1/2$; and the pre-factor is a result of the conversion from a spherical Bessel function to a Bessel function. It can be seen explicitly that the weight function is now $w(r, \nu/k) = 1$ for $\nu/k \leq r$, and $w(r, \nu/k) = 0$ for $\nu/k > r$.

The expansion of this case to higher orders can be done using equation (26), however it can be seen that the calculation is more complex than the LoVerde & Afshordi (2008) derivation because the function $f(x)$ in that equation is now $f(r'|r, k) = (\pi/2k^3r)^{1/2} w(r[z], r') [F_K(r, r')/a(r')] P^{1/2}(k, r')$. In particular the expansion does not affect the weight function evaluation $w(r, \nu/k)$ because the arguments to this do not change in the higher order terms. Also the expansion is only valid over the region $\nu/k < r$ where the derivatives of this function are not divergent.

We can now attempt to derive the standard weak lensing formulation of the Limber-approximated cosmic shear power spectrum (Kaiser, 1998) using equations (7) and (8). Substituting equation (29) we find that

$$\begin{aligned} C_\ell^{SR,L}(z_i, z_j) = & |D_\ell|^2 \mathcal{A}^2 \int \frac{dk}{k^2} \int dz_p dz' dz'_p dz'' n(z_p) n(z'_p) p(z_p|z') p(z'_p|z'') W^{SR}(z_i, z_p) W^{SR}(z_j, z'_p) \\ & \left(\frac{\pi}{2\nu k^2} \right) \frac{F(r(z'), \nu/k)}{a(\nu/k)} \frac{F(r(z''), \nu/k)}{a(\nu/k)} P(k, \nu/k) \end{aligned} \quad (30)$$

where we have absorbed the weight functions w into the integral limits for clarity, and $\mathcal{A} = 3\Omega_M H_0^2 / (2\pi c^2)$. To express this equation in the standard form we need to transform integration variables from k to r in the outer integral. This leads to

$$\begin{aligned} C_\ell^{SR,L}(z, z') = & |D_\ell|^2 \mathcal{A}^2 \left(\frac{1}{\nu^4} \right) \left(\frac{\pi}{2} \right) \int dr r^2 \int dz_p dz' dz'_p dz'' n(z_p) n(z'_p) p(z_p|z') p(z'_p|z'') W^{SR}(z_i, z_p) W^{SR}(z_j, z'_p) \\ & \frac{F(r(z'), r)}{a(r)} \frac{F(r(z''), r)}{a(r)} P(\nu/r, r), \end{aligned} \quad (31)$$

the inner integrals can now be expressed in terms of kernel functions

$$q(r_i, r) = \frac{r}{a(r)} \int dz_p dz'_p n(z_p) p(z|z_p) W^{SR}(z_i, z_p) \left(\frac{r(z') - r}{r'} \right) \quad (32)$$

where we have expanded the function F_K for the flat-geometry case ($K = 0$). Therefore the Limber-approximated power spectrum can be written as

$$C_\ell^{SR,L}(z, z') = |D_\ell|^2 \mathcal{A}^2 \left(\frac{1}{\nu^4} \right) \left(\frac{\pi}{2} \right) \int dr q(r_i, r) q(r_j, r) P(\nu/r, r). \quad (33)$$

This is the standard form for the cosmic shear power spectrum (see e.g. Hu, 1999; Joachimi & Bridle, 2009), except that the ℓ -dependent pre-factor is different. The full ℓ -mode dependent prefactor is

$$T_\ell = \frac{|D_\ell|^2}{\nu^4} = \frac{(\ell+2)(\ell+1)\ell(\ell-1)}{(\ell+0.5)^4}. \quad (34)$$

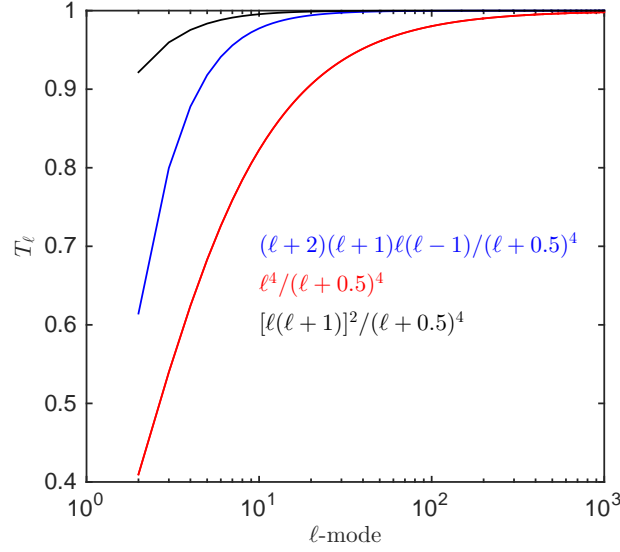


Figure 7. The functional form of the ℓ -dependent prefactor in equations (33), (34) and (35), for the cosmic shear spherical (blue) and flat-sky (red) cases, and for the convergence case (black).

In the standard derivation there are two assumptions that remove this pre-factor. These assumptions are the flat-sky approximation whereby $|D_\ell|^2 = \ell^4$, and the approximation $\nu = \ell$ (or $\ell = (\ell + 0.5)$). In this case $T_\ell = 1$ and the standard result is recovered. However these approximations can have a large impact on the amplitude of the power spectrum at $\ell \lesssim 100$ as we investigate in this paper. In Figure 7 we show the functional form of T_ℓ . To recover the correct ℓ -mode scaling from a standard cosmic shear analysis one should multiply by T_ℓ .

One can also compute a convergence power spectrum from weak lensing data. This is different from the shear case only in that the factor $D_\ell = \ell(\ell + 1)$ in the spherical-sky case. Following the derivation above we find that the Limber-approximated convergence power spectrum is the same as equation (33) but with an ℓ -dependent prefactor of

$$T_\ell^\kappa = \frac{[\ell(\ell + 1)]^2}{(\ell + 0.5)^4}. \quad (35)$$

Again, under the assumption that $\nu = \ell$ and $\ell \simeq \ell + 1$ this factor cancels, but does not in general as also noted by Joudaki & Kaplinghat (2012). We again show the effect in Figure 7, which is less pronounced than for the shear case.